Computer Methods in Biomechanics and Biomedical Engineering
Vol. 00, No. 00, October 2012, 1–

RESEARCH ARTICLE

Evaluation of the strain–line patterns in a human left ventricle: a simulation study

S. Gabriele[a], P. Nardinocchi[b]*, V. Varano[b]

[a] *Dip. di Architettura, Università Roma Tre, I-00146 Roma*
[b] *Dip. di Ingegneria Strutturale e G., Sapienza - Università di Roma, I-00184 Roma*

(*v4.1 released February 2008*)

The aim of the paper is to emphasize the role of the primary strain–line patterns in a human left ventricle within the complex system that is the heart. In particular, a protocol is proposed for the measurement of the principal strain lines (PSL) in the walls of the left ventricle; this protocol is tested by means of a computational model which resembles a human left ventricle. When the analysis is focused on the epicardial surface, PSL can be used to derive information on the directions of muscle fibers during the entire cardiac cycle, not only the systolic phase.

Keywords: strain lines, myocites architecture, left ventricle, nonlinear mechanics

1. Introduction

In structural mechanics, the stresses and strains within a body are limited above and below by their principal counterparts; this allows for the discussion and verification of the mechanical state of that body. Moreover, the principal stress and strain lines (which are the same only when special symmetry conditions are verified) determine the directions where the largest strains and/or stresses are to be expected. Due to these characteristics, the mechanics of fiber–reinforced bodies are often based on the detection of the principal strain lines and, wherever needed, fiber architecture is conceived in order to make the fiber lines coincide with the principal strain lines (PSL). Fibers make a tissue highly anisotropic; hence, principal strain and stress lines may be distinct. Whereas principal strains can be measured starting with the analysis of tissue motion, being only dependent on the three–dimensional strain state of the tissue, principal stresses can only be inferred. Thus, the PSL have a predominant role where the analysis of the mechanics of a body is concerned. Where cardiac tissues are concerned, it is worth noting that muscle fibers function as uniaxial actuators that drive tissue contraction (while collagen fibers act as the passive reinforcement of the myocardial tissue) and that it is often assumed that they share the same direction. Hence, it can be expected that, during the systolic phase, strains will mainly be suffered by highly-contracting muscle fibers and, in this case, PSL may very well agree with muscle fiber lines. Outside of this time range, the identification of strain lines is not straightforward. In addition, given that only the endocardial surface is subjected to high blood pressures, the roles of the endocardial and epicardial fibers may differ. The present

*Corresponding author. Email: paola.nardinocchi@uniroma1.it

ISSN: 1741-5977 print/ISSN 1741-5985 online

DOI: 10.1080/1741597YYxxxxxxxx
http://www.informaworld.com

paper wishes to make some progress towards improving the ability to obtain information on the fiber architecture within the heart walls thanks to the detection of the PSL. Now that full-volume images of the heart walls can be obtained by high-resolution 3-dimensional Real Time (3DRT) speckle tracking-based motion-detecting echocardiography (STE) (in short, 3DSTE), many of the shortcomings of 2D echocardiography (as opposed to NMRI) can be overcome, to the extent that myocardium strains may be investigated noninvasively with high accuracy (**???**). The goal in (**?**)is the same. Therein, the patterns of the principal strain lines on the endocardial surface of the left ventricles of a few normal adults are analyzed and discussed. The primary and secondary strain lines, corresponding to the smallest and the largest PSL, are evaluated as the outcomes of an eigenvalue analysis on a strain tensor, based on echocardiographic data. The analysis is limited to the systolic phase, evaluated as the most appropriate to infer data on the architecture of muscle fibers, and to the endocardial surface, as it has been noted that the epicardial echocardiographic data is not adequate. A qualitative similarity between the PSL and the expected pattern of muscle fibers on the endocardial surface is observed near the systolic peak. In this paper, a protocol of measurement of the PSL on the endocardial and epicardial surfaces based on data from 3DSTE is presented and discussed. The protocol is based on the evaluation of the standard strain tensor of nonlinear mechanics, directly from data acquired by 3DSTE on the positions of specific points (the *markers* of 3DSTE) at different frames during the cardiac cycle. The protocol is tested on a set of data generated by the computational model presented in (**?**) and briefly summed up in the next section. Therein, the architecture of muscle fibers in the walls of the left ventricle is included as part of the model; hence, the test allows for discussing the appropriateness of the PSL to correctly identify the directions of muscle fibers. The main conclusions of the paper are two. Firstly, the protocol delivers the strain field and the PSL on the endocardial and epicardial surface with a good approximation; secondly, it suggests that the epicardium rather than the endocardium should be analyzed to infer information on muscle fibers from 3DSTE data.

2. Background

In (**?**), a realistic geometrical model of the left ventricle (LV) is developed from data recorded through 3DSTE. The nonlinear mechanics of the LV body during a typical cardiac cycle are studied through a computational model whose outcomes are successfully compared with the strain data given by 3DSTE (see (**?**) for details of the technique). The main characteristics of the above model are briefly listed. The reference configuration $\mathcal{B}$ of the LV body is a three–dimensional region of the Euclidean space $\mathcal{E}$, corresponding to a zero–stress and no loads configuration. Of course, it does not correspond to any configuration assumed by a real LV during the cardiac cycle, and is determined by the following condition: the geometrical characteristics of the LV body at the end diastole are those of a representative subject (selected from the group of normal subjects examined in (**?**)) in the end diastolic frame. The muscle architecture is described by assigning a unit vector field $\mathbf{e} : \mathcal{B} \to \mathcal{V} = T\mathcal{E}$ representing the transmurally, linearly varying, muscle fiber direction. Denoted by β the angle between a fiber and the circumferential direction; it is assumed that $\beta = -60°$ on the epicardial surface $\partial\mathcal{B}_{epi}$ (fibers spiraling counterclockwise toward the base), and $\beta = 80°$ on the endocardial surface $\partial\mathcal{B}_{endo}$ (fibers spiraling clockwise). The displacement vector field is denoted by $\mathbf{u}$ and the deformations of $\mathcal{B}$ are described by the tensor field $\mathbf{F} = \mathbf{I} + \nabla\mathbf{u}$, where $\mathbf{I}$ is the identity tensor. Following (**?**), the deformation gradient is multiplicatively

decomposed into an active component, $\mathbf{F}_a$, describing tissue contraction and an elastic component, $\mathbf{F}_e$, describing the elastic deformation, as

$$\mathbf{F}_a = \delta\, \mathbf{e} \otimes \mathbf{e} + \left(\frac{1}{\delta}\right)^{1/2} (\mathbf{I} - \mathbf{e} \otimes \mathbf{e}) \quad \text{and} \quad \mathbf{F} = \mathbf{F}_e\, \mathbf{F}_a\,, \tag{2.1}$$

where the scalar field δ, the fiber contraction, is not constant along the cardiac cycle and is related to the fiber shortening ε by $\varepsilon = 1 - \delta$. A transversely isotropic strain energy density $\hat{\psi}$ per unit of stress-free volume is assumed to describe the passive properties of the cardiac tissue as the sum of an isotropic component $\hat{\psi}_i$ and an anisotropic component $\hat{\psi}_f$, which takes into account the fiber reinforcement (effective only for positive stretching of the fibers with respect to the contracted state), as

$$\hat{\psi}(\mathbf{C}_e) = \hat{\psi}_i(I_1(\mathbf{C}_e)) + \hat{\psi}_f(I_4(\mathbf{C}_e), I_5(\mathbf{C}_e))\,, \quad \mathbf{C}_e = \mathbf{F}_e^T\, \mathbf{F}_e\,; \tag{2.2}$$

here $I_i(\mathbf{C}_e)$ $(i = 1, 4, 5)$ are the invariants of $\mathbf{C}_e$:

$$I_1(\mathbf{C}_e) = \mathbf{I} \cdot \mathbf{C}_e\,, \quad I_4(\mathbf{C}_e) = \mathbf{C}_e\mathbf{e} \cdot \mathbf{e}\,, \quad I_5(\mathbf{C}_e) = \mathbf{C}_e^2\mathbf{e} \cdot \mathbf{e}\,. \tag{2.3}$$

Moreover, the energy function is added to an isochoric constraint on the elastic deformation guaranteeing that $\det \mathbf{C}_e = 1$. The Cauchy stress tensor reads

$$\mathbf{T} = 2\mathbf{F}\, \mathbf{F}_a^{-1} \frac{\partial \hat{\psi}}{\partial \mathbf{C}_e} \mathbf{F}_a^{-1}\, \mathbf{F}^T - p\mathbf{I}\,, \tag{2.4}$$

where p, the hydrostatic pressure field, is a direct result of the incompressibility constraint. As usual, where large deformations are concerned, the standard balance equations of forces are written in the reference configuration $\mathcal{B}$ in terms of the reference stress $\mathbf{S} = (\det\mathbf{F})\mathbf{T}\mathbf{F}^{-T}$. The boundary conditions set blood pressure π on $\partial\mathcal{B}_{endo}$ to be a scalar field varying along the cardiac cycle (see Figure 1 (right)), whereas a stress–free condition is set on $\partial\mathcal{B}_{epi}$; a torsional spring is put on the mitral annulus partially hampering the torsional motion, and the displacements along the direction of the longitudinal LV axis are constrained. Any bulk force, inertia included, is assumed negligible. In order to solve an inverse problem, a muscle contraction field δ describes a spatially uniform function varying along the cardiac cycle together with the blood pressure field π; the mechanical response of the LV body is evaluated by solving a one–parameter family of nonlinear elastic problems, where the parameter spans the cardiac cycle (**?**). Contraction and pressure along the cardiac cycle are shown in Figure 1.

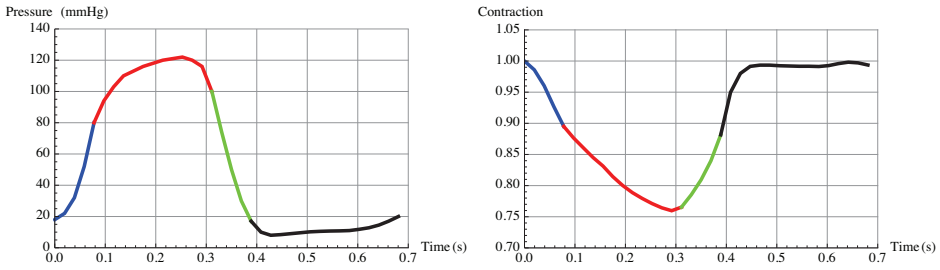

Figure 1. Pressure π (left) and contraction δ (right) along the cardiac cycle. The red portions of the lines correspond to the systolic phase within the cardiac cycle. Whereas the pressure data are real data, the contraction data have been inferred in such a way to get specific characteristics of the LV motion, so as derived from 3DSTE data (see (**?**)).

3. Method

The outcomes of the computational model set in (**?**) are therein extensively discussed; here, the attention is devoted to the (visible) strain tensor $\mathbf{C} = \mathbf{F}^T\mathbf{F}$ which collects all the information on strains suffered by the tissue. It is worth noting that the strain $\mathbf{C}$ accounts for both the active strain

$$\mathbf{C}_a = \mathbf{F}_a^T\,\mathbf{F}_a\,, \tag{3.5}$$

and the elastic strain $\mathbf{C}_e$ (see (**?**) for further details); however, it does not include any additive decomposition of the total strain $\mathbf{C}$ into its active and elastic parts, as it holds[1]

$$\mathbf{C} = \mathbf{F}_a^T\,\mathbf{C}_e\,\mathbf{F}_a\,. \tag{3.6}$$

It is to be noted that both the elastic component $\mathbf{C}_e$ and the active component $\mathbf{C}_a$ can be the dominant component of the total visible strain $\mathbf{C}$ in different crucial moments of the cardiac cycle such as the diastolic and the systolic phases, respectively, and in different parts of the myocardium, such as the epicardium and the endocardium. It is worth noting that when $\mathbf{C}_a$ prevails, it is expected that the PSL are similar to the directions of the fibers, while, in general, this is not true when $\mathbf{C}_e$ prevails. In fact, while the principal directions of $\mathbf{C}_a$ are determined by the equations (2.1) and (3.5), $\mathbf{C}_e$ is dependent on the solution of the elastic problem. It is worth highlighting that the situation in which $\mathbf{C} = \mathbf{C}_a$ (i.e. $\mathbf{C}_e = \mathbf{I}$) cannot exist because, as established in (**?**), $\mathbf{C}_a$ is not compatible, apart from the trivial case where $\delta = 1$. A preliminary analysis is firstly carried out to verify the relationships between the PSL and the muscle fiber lines within the tissue, along the whole cardiac cycle. An indicator able to quantify the similarity between PSL and muscle fiber lines is introduced and its pattern along the cardiac cycle at different points within the LV walls is discussed, with reference to the computational model developed in (**?**). Therein, the computational solution of a specific nonlinear elastic problem (where specific means that geometric and material data, as well as the muscle fiber architecture, are given) delivers primary and secondary strain lines through a simple eigenvalue analysis on $\mathbf{C}$. This nonlinear elastic solution is used to assess the role of the PSL during the whole cardiac cycle. Next, a protocol of measurement of the PSL is proposed, to be used on 3DSTE data. 3DSTE devices measure the motion of the walls, tracking the position of a set of markers, automatically set by the device's software, along the cardiac cycle. The strain tensor $\mathbf{C}$ can be evaluated accordingly. Here the protocol is exemplified with the help of the computational model. The whole procedure and the example are discussed in detail in the following sections.

3.1 Preliminary analysis

The finite collection of points identified as the vertices of the triangular elements used to discretize $\partial\mathcal{B}_{endo}$ and $\partial\mathcal{B}_{epi}$ is shown in Figure 2; they are denoted $\mathcal{D}(\partial\mathcal{B}_{endo})$ and $\mathcal{D}(\partial\mathcal{B}_{epi})$, respectively. The total visible strain tensor $\mathbf{C}$ corresponding to the solution of the previously summed up nonlinear elastic problem is known at any $X_i \in \mathcal{D}(\partial\mathcal{B}_{endo}) \cup (\mathcal{D}(\partial\mathcal{B}_{epi})$ for any contraction–pressure pairs of values

[1]The additive decomposition of strains into active and elastic components only pertain to linear theory, where the equation (3.6) is replaced by $\mathbf{E} = \mathbf{E}_e + \mathbf{E}_o$, with $\mathbf{E}$, $\mathbf{E}_e$, and $\mathbf{E}_o$ the linear visible, elastic, and active deformations respectively.

(δ_j, π_j) corresponding to a frame $j \in \mathsf{n} \subset \mathbb{N}$ along the cardiac cycle, where n is a subset of the set $\mathbb{N}$ of the natural numbers, hence a time within the characteristic interval $(0, 0.7)$ s. The pairs $(\gamma_m(X_i, j), \mathbf{c}_m(X_i, j))$ $(m = 1, 2, 3)$ of eigenvalues

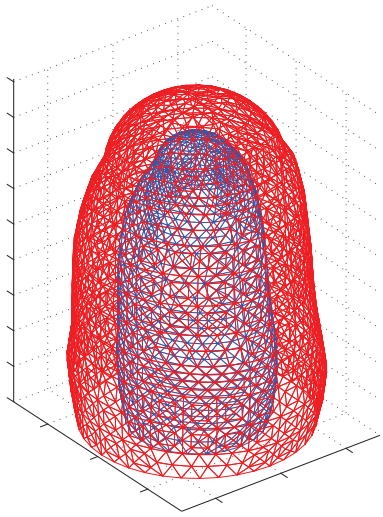

Figure 2. Representation of the discretized epicardial (red) and endocardial (purple) surfaces generated within the finite element code. The surfaces correspond to a left ventricle with a long axis of 9.8 cm, a short axis of 4.35 cm, a short axis wall thickness of $\sim$ 1 cm, and an end diastolic endocardial volume of $\sim$ 102 ml.

and eigenvectors of the strain tensor $\mathbf{C}$ can easily be evaluated. The corresponding surface strain tensor $\hat{\mathbf{C}}$ is obtained through a preliminary projection of $\mathbf{C}$ onto the epicardial and endocardial surfaces. The projector $\mathbf{P} = \mathbf{I} - \mathbf{n} \otimes \mathbf{n}$, where the field $\mathbf{n}$ corresponds to the unit normal field of the endocardial and epicardial surfaces, leads to the following definition:

$$\hat{\mathbf{C}} = \mathbf{PCP}\,. \tag{3.7}$$

The eigenvalue analysis performed on $\hat{\mathbf{C}}$ delivers the pairs of eigenvalue and eigenvector $(\hat{\gamma}_m(X_i, j), \hat{\mathbf{c}}_m(X_i, j))$ $(m = 1, 2, 3)$, where the eigenvectors are ordered by ascending eigenvalues. It is expected that $\hat{\mathbf{C}}$ will represent a plane strain state, hence, that it will have a zero eigenvalue corresponding to the eigenvector $\hat{\mathbf{c}}_1 = \mathbf{n}$; and that the primary strain lines on the (discretized) surfaces will be the streamlines of the eigenvector $\mathbf{c}_2$, which lies on the surface and corresponds to the smallest nonzero eigenvalue. To evaluate and specify the similarity between primary and secondary strain lines and the muscle bands on the endocardial and epicardial surfaces respectively, the fields $\hat{\theta}_\alpha : \mathcal{D}(\partial_{\mathcal{B}_{endo}}) \times \mathsf{n} \to \mathbb{R}$ are introduced as

$$\hat{\theta}_\alpha(X_i, j) = \arccos \hat{\mathbf{c}}_\alpha(X_i, j) \cdot \mathbf{e}(X_i)\,, \quad \alpha = 2, 3\,, \tag{3.8}$$

where $\mathbf{e}(X_i)$ is the fiber vector at the point X_i; the fields are considered to be material, assigned once for all on the reference configuration of the body. At a point $X_i \in \mathcal{D}(\partial\mathcal{B}_{endo})$ along the cardiac cycle, $\hat{\theta}_2(X_i, \cdot)$ $(\hat{\theta}_3(X_i, \cdot))$ gives the difference in orientation between the fiber line and the PSL (secondary strain lines).

3.2 The protocol for measuring strain lines

When the pattern of the PSL is derived from 3DSTE data, the starting point is very different. Typically, 3DSTE devices adopt a discretization of the LV through 36 planes perpendicular to the longitudinal axis of the LV; each plane is then divided into 36 sections along the circumference, each 10 degrees apart; this subdivision gives rise to 36×36 points on both the endocardial and the epicardial surfaces. Hence, the real LV is identified by a cloud of points p_i whose motion is followed along the cardiac cycle. The position of each of the $(36\times36)\times2$ points p_i ($i = 1, 36\times 36 \times 2$) is registered by the device at each time frame j of the cardiac cycle, and represented through the set of its Cartesian coordinates. The coordinates refer to a system represented by the $\mathbf{i}_3$ axis defined by the longitudinal LV axis and the $(\mathbf{i}_1, \mathbf{i}_2)$ axes on the orthogonal planes. The clouds of markers are intrinsically ordered. At a first level, it is possible to recognize an epicardial and an endocardial cloud, each of them consisting of 36×36 points, here named $\mathcal{S}_{epi}$ and $\mathcal{S}_{endo}$ respectively. As an example, the clouds obtained from the computational model at its reference configuration, are shown in Figure 3. Moreover, an intrinsic order within each cloud can be identified with respect to the coordinate system which implicitly is used by the device to order the points: to any marker on $\partial\mathcal{B}_{epi}$ ($\partial\mathcal{B}_{endo}$) is associated a z–position along the vertical axis and a ϕ–position on the plane crossing the longitudinal LV axis at that z. The previous discussion about the intrinsic order of the epicardial and endocardial point clouds is propaedeutic to discussing the evaluation of the strain tensor $\mathbf{C}$, as in the following. The procedure adopted to evaluate the strain tensor $\mathbf{C}$ is borrowed from classical topics in Solid Mechanics (**?**); these concern the transformation of line, area, and volume elements under a motion whose gradient at a point $X \in \mathcal{B}$ and a time t is $\mathbf{F}$. Indeed, a pair $(X, X - X_o) \in \mathcal{B} \times \mathcal{V}$, with X_o close to X, under this motion is transformed according to

$$(X, X - X_o) \mapsto (x, x - x_o)\,, \tag{3.9}$$

where x and x_o are the positions of the points X and X_o at time t, respectively; this gives

$$x - x_o = \mathbf{F}(X - X_o)\,. \tag{3.10}$$

In general, once $X \in \mathcal{B}$ is fixed and a pair of covariant and controvariant bases $\mathbf{a}_i$ and $\mathbf{a}^i$ ($i = 1, 2, 3$) are given, the following *two–point* representation of the tensor $\mathbf{F}$ respectively holds:

$$\mathbf{F} = \tilde{\mathbf{a}}_i \otimes \mathbf{a}^i\,, \quad \tilde{\mathbf{a}}_i = \mathbf{F}\mathbf{a}_i\,. \tag{3.11}$$

Hence, the mixed components of $\mathbf{F}$ can be evaluated as

$$\mathbf{F}^r{}_s = \mathbf{F} \cdot \mathbf{a}^r \otimes \mathbf{a}_s = \mathbf{F}\mathbf{a}_s \cdot \mathbf{a}^r = \tilde{\mathbf{a}}_s \cdot \mathbf{a}^r\,, \tag{3.12}$$

whatever the representation of $\mathbf{a}^r$ and $\tilde{\mathbf{a}}_s$. Following from (3.12), the strain tensor $\mathbf{C}$ turns out to be $\mathbf{C} = \mathbf{F}^T\mathbf{F}$. To each point $P \in \mathcal{S}_{epi}$ ($\mathcal{S}_{endo}$), identified within the intrinsic reference system by the pairs of 3DSTE coordinates z and ϕ, corresponds a set of n positions within the Cartesian coordinate system, where n is the number of equally spaced frames registered by the device along the cardiac cycle. Moreover, let $P_z \in \mathcal{S}_{epi}$ and $P_\phi \in \mathcal{S}_{epi}$ be the points close to the point P in the 3DSTE topology, *i.e.* identified within the intrinsic reference system by the pair $(z + h_z, \phi)$

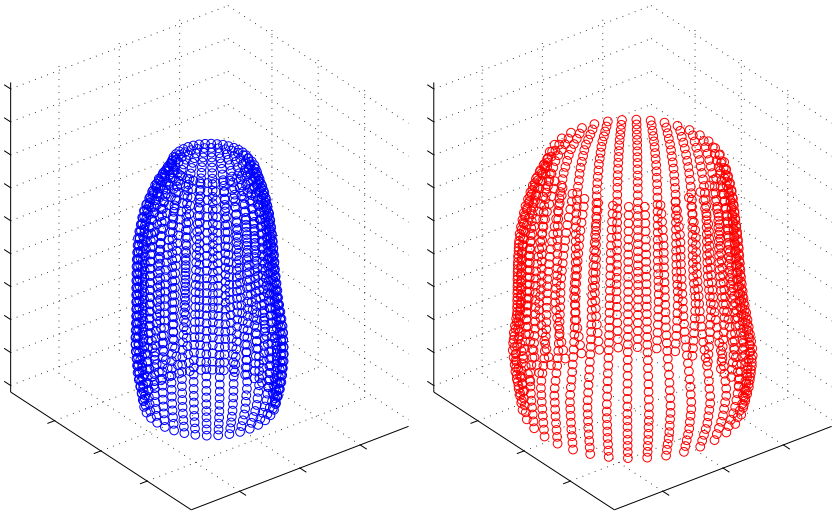

Figure 3. Endocardial (left) and epicardial (right) clouds: blue circles denote the markers $p_i \in \mathcal{S}_{endo}$ and red circles denote the markers $p_i \in \mathcal{S}_{epi}$. Both the endocardial and epicardial markers are automatically set by the device's software, once a few key markers have been selected by the medical operator.

and $(z, \phi + h_\phi)$ of 3DSTE coordinates, where $h_z = H(LV)/36$, $h_\phi = 2\pi/10$, and $H(LV)$ the height of the LV model. The vectors $P_z - P$ and $P_\phi - P$ span a non-orthonormal covariant basis $(\mathbf{a}_1, \mathbf{a}_2)$ which corresponds to the 3DSTE coordinate system. Let $\mathbf{a}_3 = \mathbf{a}_1 \times \mathbf{a}_2$, it is now possible to construct a unique non–orthogonal basis $(\mathbf{a}^1, \mathbf{a}^2)$ such that

$$\mathbf{a}^1 = \frac{\mathbf{a}_2 \times \mathbf{a}_3}{\mathbf{a}_1 \cdot \mathbf{a}_2 \times \mathbf{a}_3} \quad \text{and} \quad \mathbf{a}^2 = \frac{\mathbf{a}_3 \times \mathbf{a}_1}{\mathbf{a}_1 \cdot \mathbf{a}_2 \times \mathbf{a}_3}\,, \tag{3.13}$$

where $\mathbf{a}_1 \cdot \mathbf{a}_2 \times \mathbf{a}_3 = \mathbf{a}_3 \cdot \mathbf{a}_3$ the scalar triple product. It holds $\mathbf{a}^\alpha \cdot \mathbf{a}_\beta = \delta^\alpha_\beta$, where $\alpha, \beta = 1, 2$. Let p, p_z, and p_ϕ denote the positions occupied by the points P, P_z, and P_ϕ respectively at the frame j. The deformation gradient $\mathbf{F}$ at position P and frame j admits the following representation

$$\mathbf{F} = (p_z - p) \otimes \mathbf{a}^1 + (p_\phi - p) \otimes \mathbf{a}^2\,, \tag{3.14}$$

and its mixed components can be evaluated as

$$\mathbf{F}^\alpha_{\ \beta} = \mathbf{F} \cdot \mathbf{a}^\alpha \otimes \mathbf{a}_\beta = \mathbf{F}\,\mathbf{a}_\beta \cdot \mathbf{a}^\alpha = \tilde{\mathbf{a}}_\beta \cdot \mathbf{a}^\alpha\,, \tag{3.15}$$

where $\tilde{\mathbf{a}}_1 = (p_z - p)$ and $\tilde{\mathbf{a}}_2 = (p_\phi - p)$. Both $\tilde{\mathbf{a}}_\beta$ and $\mathbf{a}^\alpha$ are known in terms of their Cartesian coordinates. Thus, the following holds:

$$\tilde{\mathbf{a}}_1 = \lambda^z_i(j)\,\mathbf{i}_i \quad \text{and} \quad \tilde{\mathbf{a}}_2 = \lambda^\phi_i(j)\,\mathbf{i}_i\,, \tag{3.16}$$

where j refers to the frame along the cardiac cycle;

$$\mathbf{a}_1 = \lambda^z_i\,\mathbf{i}_i \quad \text{and} \quad \mathbf{a}_2 = \lambda^\phi_i\,\mathbf{i}_i\,, \tag{3.17}$$

where $\lambda^\phi_i = \lambda^\phi_i(0)$ and $\lambda^z_i = \lambda^z_i(0)$;

$$\mathbf{a}_3 = (\lambda^\phi_2\,\lambda^z_3 - \lambda^\phi_3\,\lambda^z_2)\mathbf{i}_1 + (\lambda^\phi_3\,\lambda^z_1 - \lambda^\phi_1\,\lambda^z_3)\mathbf{i}_2 + (\lambda^\phi_1\,\lambda^z_2 - \lambda^\phi_2\,\lambda^z_1)\mathbf{i}_3\,; \tag{3.18}$$

and, eventually, $\mathbf{a}^1$ and $\mathbf{a}^2$ may be evaluated from (3.13) using (3.17) and (3.18). Once the mixed components of the deformation gradient $\mathbf{F}$ have been evaluated at every point $P \in \mathcal{S}_{epi}$ ($P \in \mathcal{S}_{epi}$) and at every frame $j \in \mathsf{n}$, it is easy to obtain the total surface strain tensor, $\bar{\mathbf{C}}$

$$\bar{\mathbf{C}}_{\beta\delta} = \mathbf{F}^{\alpha}_{\ \beta}\, \mathbf{F}^{\gamma}_{\ \delta}\, (\mathbf{a}_\alpha \cdot \mathbf{a}_\gamma)\,. \tag{3.19}$$

The eigenvalue analysis should reveal a plane strain state, thus delivering the expected results concerning the primary and secondary strain lines. The corresponding eigenvalue–eigenvector pairs are denoted as $(\bar{\gamma}_\alpha, \bar{\mathbf{c}}_\alpha)$, where $\alpha = 2, 3$.

Remark. The proposed protocol is based on the evaluation of the positions occupied by the points along the cardiac cycle in their corresponding Cartesian coordinates. These coordinates, once real 3DSTE data is analyzed, will be directly identified by the system. So far, the intrinsic 3DSTE topology has only been used to define the closeness between points in the configuration (hence, at the frame) chosen as reference, and to obtain a special two–point representation of the deformation gradient tensor. Moreover, the evaluation of the nonlinear strain tensor $\mathbf{C}$ is performed in one *derivative* step, which relates to the position of points that are close to each other in the 3DSTE topology. Other techniques have been proposed (**?**); these define the strain tensor as the integral of the strain rate tensor which is determined from the gradient of material velocity measures. Hence, these techniques involve two separate *derivative* steps (in space and in time) and an additional integration step (in time).

4. Results and Discussion

Firstly, the role of the pairs of eigenvalues and eigenvectors of the strain tensor $\hat{\mathbf{C}}$ evaluated on the endocardial and epicardial surfaces is discussed. In the computational model, the muscle fiber architecture is known and identified as the structure of the passive reinforcement fibers. These assumptions lead to a straightforward discussion of the relationship between the eigenvectors of the surface strain tensor $\hat{\mathbf{C}}$ and the muscle fiber lines, at different times along the cardiac cycle. When the end systolic peak time (from Figure 1, $t \simeq 0.3$ s) is selected in the (simulated) cardiac cycle, the three eigenvectors can be shown by means of their corresponding streamlines. The following Figure **??** displays the endocardial (top row) and epicardial (bottom row) surfaces, rendered by triangular meshes. At any node X_i of the mesh, the eigenvector fields $\hat{\mathbf{c}}_i$ have been highlighted, where i goes from 1 to 3, from left to right. The figure displays two remarkable findings. As expected, with $\hat{\mathbf{C}}$ a plane strain tensor, the first eigenvector $\hat{\mathbf{c}}_1$ (bottom and top left panels) has eigenvalue zero and is orthogonal to both surfaces. Moreover, the primary and secondary strain lines (which correspond to the streamlines with the smallest eigenvalues between $\hat{\gamma}_2$ and $\hat{\gamma}_3$) on the epicardial surfaces (bottom center and bottom right panels) follow the muscle fiber lines and the corresponding orthogonal lines. In the end, on the endocardial surface, the primary lines (top center panel) are circumferential and the corresponding secondary lines (top right panel) are almost aligned with the directions of the muscle fibers on the endocardial surface ($\sim 80°$). This result is justified: due to the high blood pressure during the systolic phase, the relevant total visible strains on the endocardial surface are mainly elastic and highlight circumferential bands of smallest strains. Hence, with reference to the equation (3.6), at the systolic peak the main component of $\mathbf{C}$ is the elastic component $\mathbf{C}_e$. On the contrary, on the epicardium, where pressure is extremely low,

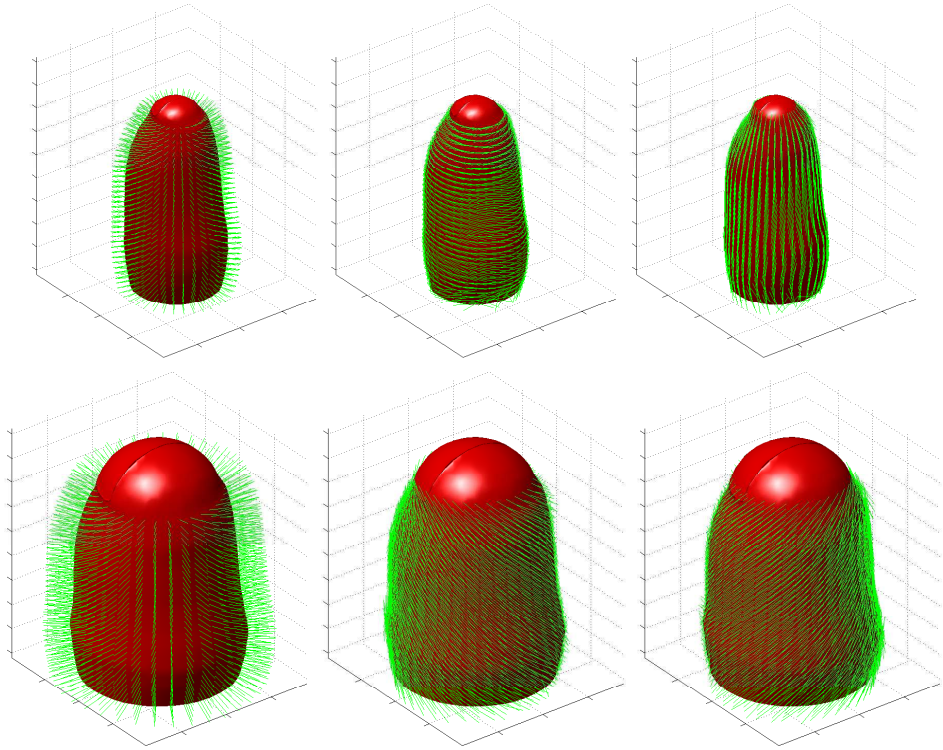

Figure 4. Representation of the epicardial (bottom row) and endocardial (top row) surfaces as generated within the finite element code. At the time corresponding to the end systole, the $\hat{\mathbf{c}}_i$ fields with $i = 1, 2, 3$ are represented by green arrows at each node, and defined the strain eigenvectors at that node.

strains are mainly active strains ($\mathbf{C}_a$) and the PSL actually suggest the orientation of the muscle fibers. These facts must be taken into account when muscle fiber architecture is unknown, as is the case when real 3DSTE data are examined. Figure **??** shows the pattern of the eigenvalues corresponding to the primary (left) and secondary (right) strain lines at each point of the mesh (red lines) and the corresponding spatial average pattern, along the entire cardiac cycle. It is worth noting that a well-defined pattern of values can be identified for both surfaces; hence, the average blue line bears meaning. At t=0, the values attained by the eigenvalues belong to the end–diastolic state. At the peak systolic frame, both first and second eigenvalues are on average less than 1; this denotes tissue shortening in the endocardium. The second step is to validate the assumption that the strain tensor $\bar{\mathbf{C}}$, that is derived from the application of the protocol proposed in the previous section and defined in equation (**??**), is suitable to obtain the same results that in our case are obtained from $\hat{\mathbf{C}}$. $\bar{\mathbf{C}}$ is hence calculated by simulating the pseudo–experimental 3DSTE data (i.e. the $p_i \in \mathcal{S}_{endo}, \mathcal{S}_{epi}$ coordinates at each step frame of the cardiac cycle, that are the unique available dataset from real human LV) from the model and by applying the protocol. The strength of the proposed protocol is assessed through a comparison of the eigenvalues $\bar{\gamma}_\alpha$ corresponding to the primary and secondary strain lines, as Figure **??** shows. The results simulated from the computational model are analogous to those obtained with the pseudo-experimental 3DSTE data. Even if not pictured, the resulting eigenvectors $\bar{\mathbf{c}}_\alpha$ equal, in practice, the $\hat{\mathbf{c}}_\alpha$ represented in Figure **??**. The last step of this discussion relates to the quantification of the similarity between the calculated eigenvectors and the directions of the fibers. As previously discussed from a qualitative point of view, the directions of the PSL differ, at the systolic peak, from endocardium to epicardium. Now, this difference is quantified along the entire cardiac cycle. Recalling the scalar fields previously defined in equation 3.8, the similarity between PSL and muscle

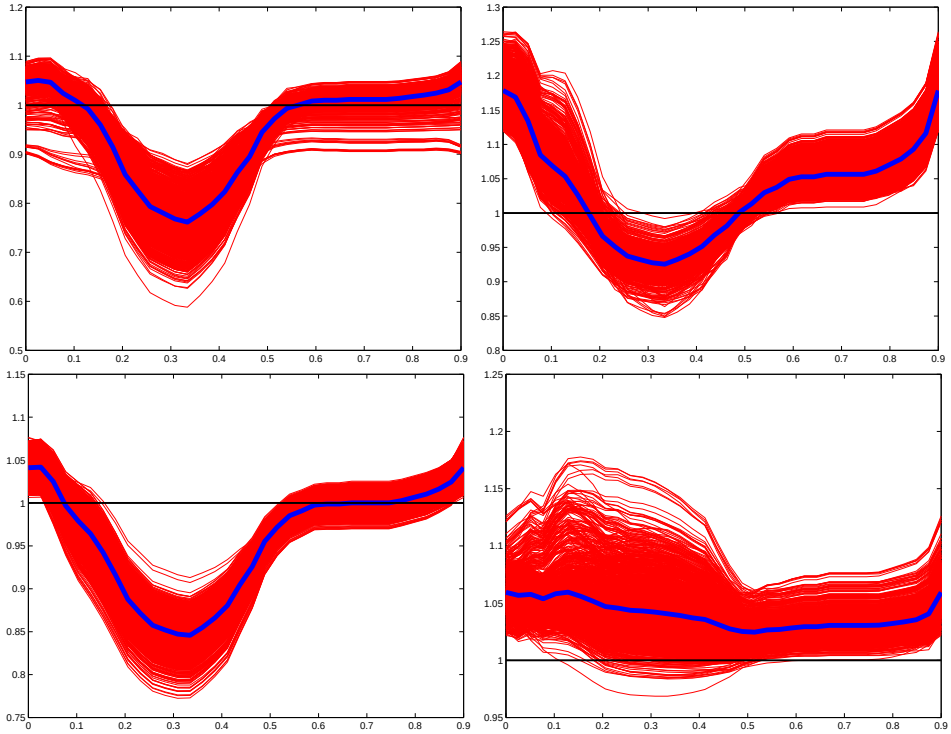

Figure 5. Eigenvalues $\hat{\gamma}_\alpha$ ($\alpha = 2, 3$) corresponding to the primary (left panels) and secondary (right panels) strain lines at each point (red lines) of the clouds $\mathcal{S}_{endo}$ (top line) and $\mathcal{S}_{epi}$ (bottom line): below the straight black line (which denotes the unit value) shortening occurs, above the line elongation occurs. The blue line identifies the spatial mean value.

fiber lines can be quantified through the introduction of the equivalent fields, now calculated over the points belonging to the protocol sets $\mathcal{S}_{endo}$ and $\mathcal{S}_{epi}$ as

$$\bar{\theta}_\alpha(X_i, j) = \arccos \bar{\mathbf{c}}_\alpha(X_i, j) \cdot \mathbf{e}(X_i)\,, \quad \alpha = 2, 3\,; \tag{4.20}$$

the same holds for $\mathcal{S}_{epi}$. When $\bar{\theta}_2 \sim 0$, the PSL and the muscle fiber lines are almost aligned; when $\bar{\theta}_2 \sim 90°$, they are almost orthogonal (and similarly for $\bar{\theta}_3$). Figure **??** shows both fields for $\alpha = 2, 3$ for the epicardial surface (left) and for the endocardial surface (right). It is evident from the figure that: (**i**) on the epicardium (right panel) the PSL and the direction of the muscle fibers are very similar, i.e. along a large part of the cardiac cycle phase the angle $\bar{\theta}_2$ is less than 20° (blue line); on the contrary, the secondary strain lines remain almost orthogonal to the same direction of muscle fibers (cyan line); (**ii**) on the endocardium (left panel), at the systolic phase when high internal blood pressures are expected, the primary strain lines (blue line) are circumferential, that is, almost orthogonal to the direction of the muscle fibers. However, it is to be noted that before blood pressure increases, that is, at the initial end–diastolic time, the PSL are very similar to the direction of the muscle fibers.

5. Conclusions

A protocol of measurement of the primary strain lines in the left ventricle's walls is proposed and tested against a computational model. The interesting result is that, provided a proper time interval is chosen, the PSL may be used to retrieve information on the direction of the muscle fibers, both for the epicardial and for the endocardial surfaces. In particular, if the analysis is limited to the epicardial surface

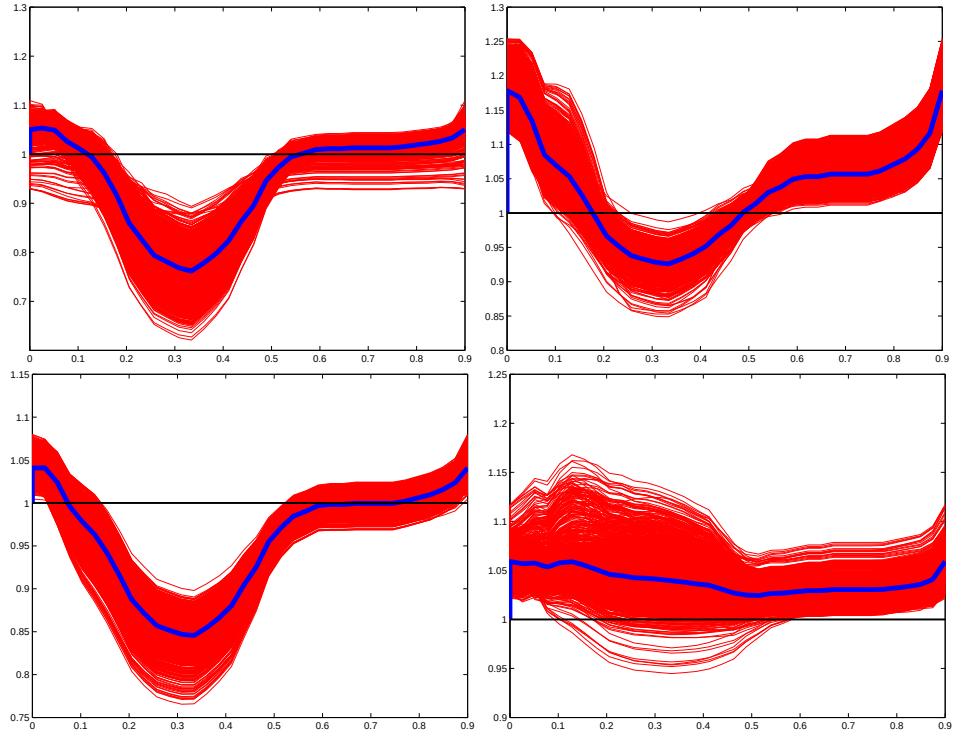

Figure 6. Eigenvalues $\bar{\gamma}_\alpha$ ($\alpha = 2, 3$)corresponding to the primary (left panels) and secondary (right panels) strain lines at each point (red lines) of the clouds $\mathcal{S}_{endo}$ (top row) and $\mathcal{S}_{epi}$ (bottom row), as evaluated by the measurement protocol.

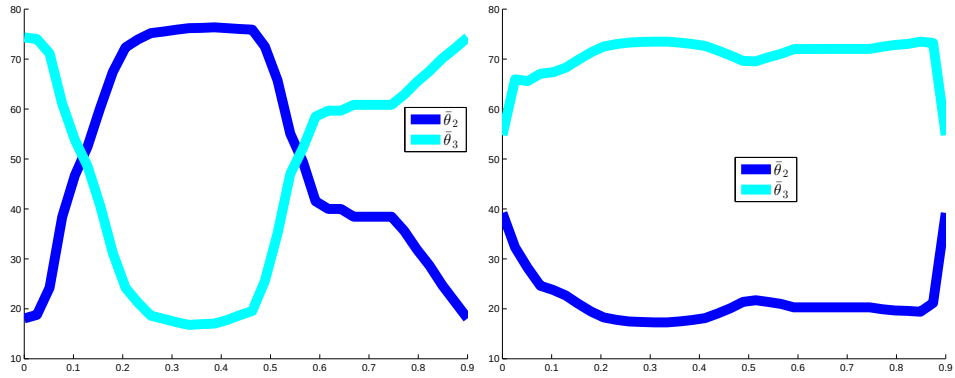

Figure 7. Spatially-averaged time–pattern of the fields $\bar{\theta}$ on the endocardial (left) and epicardial (right) surfaces.

then most of the cardiac cycle can be selected. On the contrary, the directions of the endocardial fibers can only be recovered from the first time frames of the cardiac cycle. This last result opens the road to a systematic study which can be carried on through the analysis of 3DSTE data from both normal humans and patients showing different levels of cardiac diseases. The study can help shed light on how the patterns of PSL within the walls of the left ventricle are altered in the presence of cardiac diseases.

Acknowledgements

The work is supported by MIUR (the Italian Ministry of University and Research) through the Project PRIN2009 “Mathematics and Mechanics of Biological Assemblies and Soft Tissues” and by Sapienza - Universitá di Roma through the grant N. C26A11STT5.

References

Evangelista A, Nesser J, De Castro S, Faletra F, Kuvin J, Patel A, Alsheikh–Ali AA, Pandian N. 2009. Systolic wringing of the left ventricular myocar- dium: characterization of myocardial rotation and twist in endocardial and midmyocardial layers in normal humans employing three-dimensional speckle tracking study. J. Am. Coll. Cardiol. 53(A239):1018–1268 (Abstract).

Evangelista A, Nardinocchi P, Puddu PE, Teresi L, Torromeo C, Varano V. 2011. Torsion of the human left ventricle: Experimental analysis and computational modeling. Prog. Biophys. Mol. Biol. 107(1):112–121.

Goffinet C, Chenot F, Robert A, Pouleur AC, le Polain de Waroux JB, Vancrayenest D, Gerard O, Pasquet A, Gerber BL, Vanoverschelde JL. 2009. Assessment of subendocardial vs. subepicardial left ventricular rotation and twist using two dimensional speckle tracking echocardiography comparison with tagged cardiac magnetic resonance. Eur. Heart J. 30:608–617.

Gurtin ME, 1981. An Introduction to Continuum Mechanics. Academic Press.

Helle-Valle T, Crosby J, Edvardsen T, Lyseggen E, Amundsen BH, Smith HJ, Rosen BD, Lima JAC, Torp H, Ihlen H, Smiseth OA. 2005. New noninvasive method for assessment of left ventricular rotation: speckle tracking echocar- diography. Circulation 112:3149–3156.

Maffessanti F, Nesser HJ, Weinert L, Steringer-Mascherbauer R, Niel J, Gorissend W, Sugeng L, Lang RM, Mor-Avi V. 2009. Quantitative evaluation of regional left ventricular function using three-dimensional speckle tracking echocardiography in patients with and without heart disease. Am. J. Cardiol. 104:1755–1762.

Nardinocchi P, Teresi L. 2007. On the active response of soft living tissues. J. Elast. 88: 27–39.

Nardinocchi P, Teresi L, Varano V. 2011. A simplified mechanical modeling for myocardial contractions and the ventricular pressure–volume relationships. Mech. Res. Commun. 38: 532-535.

Nardinocchi P, Teresi L, Varano V. 2012. Strain Induced Shape Formation in Cylindrical Tubes, J. Mech. Phys. Solids 60:1420–1431.

Nardinocchi P, Teresi L, Varano V. The elastic metric: A review of elasticity with large distortions, Int. J. Non-Linear Mech. (2013), http://dx.doi.org/10.1016/j.ijnonlinmec.2013.05.002i.

Pedrizzetti G, Kraigher-Krainer E, De Luca A, Caracciolo G, Mangual JO, Shah A, Toncelli L, Domenichini F, Tonti G, Galanti G, Sengupta PP, Narula J, Solomon S 2012. Functional Strain-line Pattern in the Human Left Ventricle. PRL 109:048103.